*J. Fluid Mech.* (1986), *vol.* 170, *pp.* 545–564
*Printed in Great Britain*



# Studies of the wall shear stress in a turbulent pulsating pipe flow

By ZHUO-XIONG MAO AND THOMAS J. HANRATTY
University of Illinois, Urbana, Illinois 61801, USA

(Received 13 August 1984 and in revised form 19 February 1986)

Measurements are presented of the time variation of the wall shear stress caused by the imposition of a sinusoidal oscillation on a turbulent pipe flow. The amplitude of the oscillation is small enough that a linear response is obtained and the dimensionless frequency, $\omega^+ = \omega\nu/u^{*2}$, is large compared with that studied by most previous investigators. The most striking feature of the results is a relaxation effect, similar to that observed for flow over a wavy surface, whereby the phase angle characterizing the temporal variation of the wall shear stress undergoes a sharp change over a rather narrow range of $\omega^+$. At $\omega^+$ larger than the median frequency of the turbulence there appears to be an interaction between the imposed flow oscillation and the turbulence fluctuations in the viscous sublayer, which is not described by present theories of turbulence.

## 1. Introduction

The imposition of a sinusoidal oscillation on the mean flow through a circular pipe causes a periodically varying pressure and velocity field. If the amplitude is small enough a linear response is obtained for which

$$\frac{\mathrm{d}p}{\mathrm{d}x} = \frac{\mathrm{d}\bar{p}}{\mathrm{d}x} + \left|\frac{\mathrm{d}\hat{p}}{\mathrm{d}x}\right| \cos(\omega t), \tag{1}$$

$$u = \bar{u}(y) + |\hat{u}(y)| \cos(\omega t + \Theta_u(y)), \tag{2}$$

with $x$ being the distance in the flow direction, $y$ the distance from the wall, $\omega$ the angular frequency, and $t$ the time. The time-mean pressure gradient and the time-mean velocity of the undisturbed flow are designated by $\mathrm{d}\bar{p}/\mathrm{d}x$ and $\bar{u}(y)$; and the amplitudes of the oscillations by $|\mathrm{d}\hat{p}/\mathrm{d}x|$ and $|\hat{u}(y)|$. These oscillations in the velocity field give rise to oscillations in the shear stress at the wall,

$$\tau_w = \bar{\tau}_w + |\hat{\tau}_w| \cos(\omega t + \Theta_{\tau_w}), \tag{3}$$

with $\Theta_{\tau_w} = \lim_{y\to 0} \Theta_u(y)$, as can be shown by differentiating (2). This paper presents the results of experiments with a fully developed pipe flow in which $|\hat{\tau}_w|$ and $\Theta_{\tau_w}$ are related to $|\mathrm{d}\hat{p}/\mathrm{d}x|$ (Mao 1984).

The experiments were conducted at high enough frequencies that fluid inertia is dominant over most of the flow field and the profile of the disturbance velocity is flat over the central regions of the pipe. This is confirmed by the recent experiments of Binder *et al.* (1985) at $\omega^+/15 = 0.00017$ and by numerical solutions of (11) for all of the models discussed in §3. In this central region of the pipe where fluid inertia is dominant the plug flow disturbance is described by the equation

$$\rho \frac{\partial \tilde{u}}{\partial t} = -\frac{\partial \tilde{p}}{\partial x}. \tag{4}$$

A solution of (4) for a sinusoidally varying pressure gradient gives

$$\omega\rho|\hat{u}| = \left|\frac{\mathrm{d}\tilde{p}}{\mathrm{d}x}\right|, \tag{5}$$

and a phase angle relative to the favourable oscillating pressure gradient of

$$\Theta_u = -\tfrac{1}{2}\pi. \tag{6}$$

Equation (5) reveals that, for this high frequency range, even small oscillations in the volumetric flow can cause oscillations in the pressure gradient many times larger than the mean pressure gradient.

Close to the wall turbulent and viscous stresses become important so that $u$ is related to the pressure gradient through the equation

$$\rho\frac{\partial u}{\partial t} = -\frac{\partial p}{\partial x} + \mu\frac{\partial^2 u}{\partial y^2} + \frac{\partial \tau^{(t)}}{\partial y}. \tag{7}$$

The principal theoretical problem in predicting how the oscillations in the wall shear stress are related to the oscillations in the pressure gradient is the determination of how an oscillating pressure gradient affects the turbulence. The experiments therefore provide a test of closure methods that predict $\tau^{(t)}$ close to a wall.

The motivation for this work has come from studies of the wall-shear-stress variation along a solid wavy surface over which a turbulent fluid is flowing. It was found in these experiments that the amplitude and phase angle characterizing the periodic spatial variation of the shear stress along the wavy surface depend on the wavenumber $\alpha = 2\pi/\lambda$. Of most interest was the discovery of a sharp change in phase angle $\Theta_{\tau_w}$ at a value of the dimensionless wavenumber, $\alpha^+ = \alpha\nu/u^*$, approximately equal to 0.0005–0.001.

Thorsness, Morrisroe & Hanratty (1978) and Abrams & Hanratty (1985) have suggested that this observed behaviour of the phase angle is primarily associated with the influence of the wave-induced variation of the pressure gradient. They argue that at small $\alpha^+$ an equilibrium exists whereby the flow behaves similarly to that observed in gradually expanding or converging channels. Regions of the wave surface with a favourable pressure gradient experience a damping of the turbulence in the viscous wall region; regions with an unfavourable pressure gradient experience an enhancement of the turbulence. As $\alpha^+$ increases the pressure gradient varies so rapidly along the wave surface that the turbulence in the viscous wall region cannot assume such an equilibrium condition. The sharp change in the phase angle with increasing $\alpha^+$ that is observed is a manifestation of the relaxation from an equilibrium to a frozen turbulence (for which the wave-induced flow is described approximately by a quasi-laminar assumption).

The principal goal of the present experiments was to investigate the above interpretation by carrying out studies of the influence of a rapidly varying pressure gradient (in time) on the behaviour of the viscous wall region, without having to deal with additional complications associated with streamline curvature that exists for flow over a wavy surface. Of particular interest is the determination of whether the variation of $\Theta_{\tau_w}$ with $\omega^+$ ($= \omega\nu/u^{*2}$) shows the same relaxation phenomenon observed for flow over wavy surfaces.

In order to meet the above objective it was necessary to design the experiment so that $\omega^+$ was of the same order as the median frequency; that is the frequency below which the turbulent velocity fluctuations in the vicinity of the wall contain 50% of the energy, $\omega^+ = 0.009 \times 2\pi$ (see Hanratty, Chorn & Hatziavramidis 1977).

At the same time, it was desirable to avoid the requirement of imposed oscillations of unrealistically high frequency. This was done by using a system which has low-frequency turbulence; i.e. water flow in a 19.4 cm pipe. Sinusoidal oscillations with frequencies of 0.325 and 0.625 Hz were introduced into the system with a plunger-type pump. The amplitudes of the oscillations were made small enough that the pressure gradient and wall shear stress varied sinusoidally with time. The shear-stress variation at the wall was measured with electrochemical probes mounted flush with the wall. It was not possible to design this experiment so that the frequency response of the probe did not have to be taken into account. An advantage of using the electrochemical method is that an analytical, rather than an experimental, scheme can be used to correct for frequency response.

A number of previous investigators have studied the influence of controlled flow oscillations on turbulent flows. An excellent review has recently been presented by Carr (1981). The work presented in this paper differs in that attention is focused on the wall-shear-stress variation and on high values of $\omega^+$. Previous investigators have found that the influence of the oscillations on the mean velocity profile is small and that their effect on turbulence is felt principally in the region close to the wall. For this reason, there exists a need for measurements of the wall-shear-stress oscillations. In most previous studies accurate velocity measurements were not made close enough to the wall to determine the time-varying velocity gradient at the wall. Recently, Ramaprian & Tu (1983) reported on direct measurements of the wall shear stress with flush-mounted wall-heat-transfer probes. These were at values of $\omega^+$ too low to observe the relaxation phenomenon in which we are interested. In addition, there are uncertainties about these results since no attempt was made to take into account the frequency response of the probe.

## 2. Description of experiments

### 2.1. *Experimental flow loop*

A schematic drawing of the loop in which the experiments were performed is shown in figure 1. Details regarding its design may be found in Sirkar (1969) and Sirkar & Hanratty (1970). The mean flow was generated by a centrifugal pump while the imposed oscillation was introduced by a piston with a diameter of 6.35 cm and a stroke length adjustable from 0 to 15.2 cm. The mean flow rate was measured by a vortex-shedding flow transmitter (Eastech, Model 2420) with an accuracy of 0.5%. The frequency of oscillation in the experiment was fixed at 0.325 or 0.625 Hz by adjusting the circular frequency of the motor driving the piston. The oscillating flow component was introduced into the system between diaphragm valve 3 and calming section 4. The uniform flow that emerges from the calming section is tripped by a 1.26 cm long ring consisting of a series of 0.95 cm equilateral triangles around the circumference of the entrance of the 19.4 cm pipe. In the experiment, diaphragm valve 3 and bypass valve 17 were adjusted to impose a large pressure drop across them. This minimized the distortions of the sinusoidal oscillation in the 19.4 cm pipe caused by the time response of the whole system. The flow oscillation at the centre of the pipe was calculated, using (5), from the measured time variation of the pressure gradient, as described in §2.3.

A rectangular platinum electrode was mounted flush with the wall of a test section and located 67.5 pipe diameters downstream from the pipe entrance. The size of the electrode was $0.00762 \times 0.102$ cm with its longer side perpendicular to the mean flow direction. The fluid was an aqueous solution, 0.1 M in potassium iodide and 0.0038 M

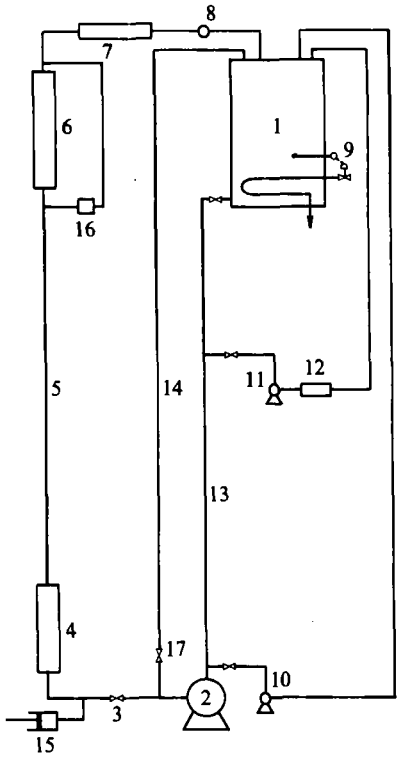


FIGURE 1. Schematic of 19.4 cm flow loop. 1, Storage tank; 2, Worthington pump; 3, Diaphragm valve; 4, Calming section; 5, 19.4 cm pipe upflow; 6, Test section; 7, Anode; 8, Vortex flow meter; 9, Temperature control unit; 10, Recycling pump; 11, Filter pump; 12, Filter; 13, 10.2 cm pipe downflow; 14, 10.2 cm bypass pipe; 15, Pulsating generator; 16, Pressure transducer; 17, Bypass valve.

in iodine, maintained at a temperature of $25 \pm 0.1$ °C. The kinematic viscosity of the solution was 0.00866 cm$^2$/s.

### 2.2. *Electrochemical technique*

When a voltage is applied to an electrochemical cell in an aqueous solution of potassium iodide and iodine, the following reactions are carried out on the surfaces of the electrodes:

$$\begin{aligned} &\text{Cathode} \quad I_3^- + 2e \rightarrow 3I^-, \\ &\text{Anode} \quad 3I^- \rightarrow I_3^- + 2e. \end{aligned}$$

When the electrochemical process is controlled by the rate of mass transfer at the surface of the cathode (the test electrode) the current flowing in the cell $I$ is related to the rate of mass transfer $N$ by the equation

$$N = \frac{I}{A_e n_e F}, \tag{8}$$

where $A_e$ is the area of the test electrode, $n_e$ the number of the electrons involved in the reaction and $F$ Faraday's constant.

From a mass balance, the mass transfer rate per unit area $N$ is related to the

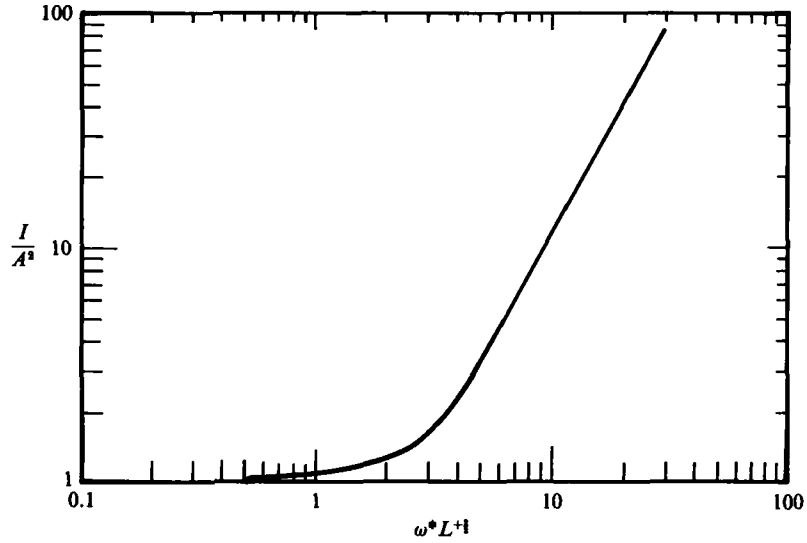


FIGURE 2. Correction factor of amplitude for time frequency response. ($A = \hat{k}_s/|\hat{k}|$, where $|\hat{k}|$ is the amplitude of time-varying transport coefficient and $\hat{k}_s$ the amplitude calculated by pseudosteady approximation. $\omega^* = \omega^+ Sc^{\frac{1}{4}}$, where $Sc$ is Schmidt number.)

velocity gradient $S$ at the surface of the test electrode. If a pseudosteady approximation is made, the solution is given by

$$K = 0.807\left(\frac{\alpha^2 S}{L}\right)^{\frac{1}{3}}, \tag{9}$$

and $N = KC_B$, where $K$ is the mass transfer coefficient, $\alpha$ the diffusivity, $L$ the length of the electrode and $C_B$ the bulk concentration of the reacting species. Equation (9) is normally used to obtain the velocity gradient at the wall, or wall shear stress, from the measured values of $K$. Details regarding the measurement of the current and the electrochemical technique are given in a review article by Hanratty & Campbell (1983).

When this technique is applied to unsteady flows, especially at high frequencies, the pseudosteady approximation might not hold. Fortuna & Hanratty (1971) considered the effect of the frequency response of the concentration boundary layer on the measured amplitude of the fluctuating flow by solving a linearized form of the time-varying conservation equation. In the present work, particular attention was given to the phase-lag errors that arise in using (9) to calculate the time variation of $\tau_w(t)$. Extensive numerical and experimental studies on this problem, summarized in a recent paper by Mao & Hanratty (1985), were carried out before doing the studies reported in this paper. Figures 2 and 3 give the corrections of the measured amplitudes and phases that need to be used. These results indicate that it is impossible to design an experiment for which the use of pseudosteady solution (9) would not introduce errors in the determination of the phase of $\tau_w(t)$, when the frequency of the imposed oscillation is of the same order as the characteristic frequency of turbulent fluctuations. Therefore, the wall-shear-stress data were first obtained by using (9), and then corrected according to figure 3.

The dimensionless probe width was $w^+ = 8.6$. This is small enough for the spatial averaging of the turbulence not to be limiting (Hanratty 1983).

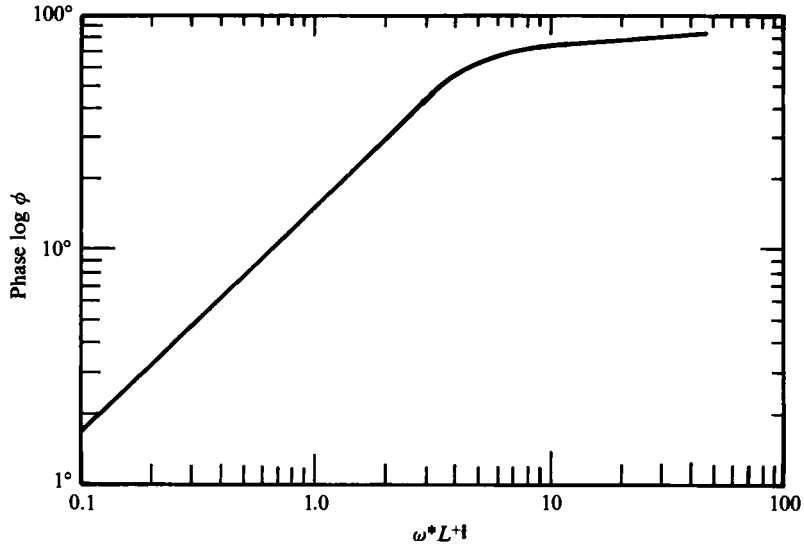


FIGURE 3. Phase lag due to time frequency response. (Phase lag $\phi$ means that the measured time-varying transport coefficient $k$ lags wall shear stress by $\phi$ due to time frequency response.)

### 2.3. *Differential pressure measurement*

Since there was a slight difference between the phase and the amplitude of the flow oscillation in the test section and the motion of the pulse generator, it was necessary to measure the flow oscillation directly in the test section. This was done with a differential pressure transmitter (Viatran Model 704-115) having a full scale $\pm 2.54$ cm water column corresponding to $\pm 5$ V output. Two pressure taps, 437.4 cm apart, were located on the two ends of the test section.

For a fully developed pipe flow, the pressure gradient $\partial p/\partial x$ is a function only of time. That is

$$\frac{\partial p}{\partial x} = \frac{\Delta p}{\Delta x}(t). \tag{10}$$

This measured time variation of the pressure gradient was used, together with equation (4), to calculate the time variation of the velocity at the centre of the pipe.

The dynamic response of the pressure transmitter was determined in the following way: the flow loop was first filled with the solution, then the flow in the 19.4 cm pipe was oscillated by the motion of the piston with diaphragm valve 3 completely closed. Because of the incompressibility of the fluid, the motion in the test section was in phase with the piston and the amplitude of the pressure-gradient variation could be calculated from the piston stroke length and frequency. The instantaneous differential pressure signals were sampled and processed as described in the next section. Several frequencies and stroke lengths were tested. It was found that the phase lag of the pressure transmitter was dependent on frequency. It was 9° for a frequency of 0.325 Hz and 25° for 0.625 Hz. The amplitude correction was dependent on $L_s f^2$, where $L_s$ is the stroke length of the pump. The differential pressure measurement, corrected in this manner, served as a standard for characterizing the imposed oscillation.

The time-mean pressure gradient was very small, so it was not possible to compare

those for steady flow and pulsating flows. The time-mean pressure gradient was calculated from the Blausius formula, assuming no effect of oscillation on the mean pressure gradient. This assumption is supported by the measurements of the time-mean wall shear stress, described in §4.

### 2.4. *Data sampling and processing*

The analog signals from the wall probes and the pressure transmitter were digitized by a 12-bit A/D converter and sampled by a minicomputer (Digital Equipment Corporation LSI-11). The time-mean shear stress and intensity were sampled at a rate of 20 Hz. A total of 2000 data points were taken for each run.

An optointerruptor on the pulse generator was used to provide a pulse of 4 V when the piston reached a certain position in each cycle. This pulse served as a phase reference. The time between the two consecutive pulses is the period of the oscillation. It was measured with a programmable timer (Berkeley 6401) and sampled through a real-time clock board in the computer. Drift of the period of different cycles was found to be less than 0.1%. For each cycle of oscillation, this pulse initiated data sampling. Thirty-two or sixty-four samples per cycle were taken in equal time intervals and a total of 500 periods of data were collected on the disc of the computer in each experiment. At each sampling point the probes and the pressure transmitter were sampled at a high enough speed that the measurements, for all practical purposes, could be considered simultaneous.

The recorded data were phase averaged. The amplitude and the phase of the velocity gradient at the wall were obtained by a least-square fit of the phase-averaged data with a cosine function.

The spectrum of the turbulent fluctuations of the velocity gradient at the wall was obtained by a fast Fourier transformation (FFT) (Bendat & Piersol 1971). The analog signals from the wall probe were filtered by an analog low-pass filter with a cutoff frequency of 20 Hz before they were sampled by the computer at a rate of 40 Hz. The cutoff frequency was much higher than the median frequency, $f^+ = 0.009$ (see Hanratty *et al.* 1977). For example, it is only about 0.6 Hz at $Re = 30000$. Therefore, turbulent fluctuations with frequencies higher than the cutoff frequency make a negligible contribution to the total energy (Hanratty *et al.* 1977). The actual sample size for each FFT was 512. A total number of 20480 of data points were used, i.e. 40 realizations were averaged to give an estimated spectrum.

### 2.5. *Experimental range*

The experiments were designed to cover a range of oscillation frequencies around the median frequency of the turbulent velocity fluctuations in the vicinity of the wall, i.e. $\omega^+ = 2\pi \times 0.009$. This was realized by fixing the frequency of the imposed oscillation at 0.625 or 0.325 Hz and varying the Reynolds number of the mean flow from 15000 to 70000. The amplitude of the central velocity variation was 10% of the mean velocity for most of the experiments. However, for high Reynolds numbers, an amplitude of less than 10% had to be used because of the limited capacity of the pulse generator. An oscillation amplitude of 5% was also used at Reynolds numbers of 15000 and 20000 with a frequency 0.625 Hz in order to examine the assumption of a linear response of the wall shear stress to the imposed oscillation. The reason for using a small amplitude was to eliminate nonlinear effects and, therefore, to make the analysis of the results easier. The experimental conditions are listed in table 1. Several dimensionless groups of frequency are also calculated for comparison with studies of other researchers.

| $Re$ | $f(s^{-1})$ | $L_s$ (cm) | $\lvert\hat{u}_c\rvert/\bar{u}_b$ | $\Omega=\left(\frac{w}{\nu}r_0\right)^{\frac{1}{2}}$ | $\frac{\omega D}{u^*}$ | $\frac{\omega D}{\bar{u}_b}$ | $\frac{\omega^+}{15}$ |
|---|---|---|---|---|---|---|---|
| 15000 | 0.325 | 8.7 | 0.1 | 149 | 99 | 5.9 | 0.0074 |
| 20000 | 0.325 | 8.2 | 0.1 | 149 | 77 | 4.4 | 0.0045 |
| 30000 | 0.325 | 11.9 | 0.1 | 149 | 54 | 3.0 | 0.0023 |
| 40000 | 0.325 | 12.7 | 0.077 | 149 | 40 | 2.2 | 0.0013 |
| 50000 | 0.325 | 12.7 | 0.062 | 149 | 35 | 1.8 | 0.0009 |
| 60000 | 0.325 | 12.7 | 0.052 | 149 | 29 | 1.5 | 0.00065 |
| 70000 | 0.325 | 12.7 | 0.044 | 149 | 26 | 1.3 | 0.00050 |
| 15000 | 0.625 | 3.2 | 0.1 | 207 | 190 | 11.4 | 0.014 |
| 20000 | 0.625 | 4.3 | 0.1 | 207 | 148 | 8.53 | 0.0086 |
| 30000 | 0.625 | 6.4 | 0.1 | 207 | 104 | 5.69 | 0.0042 |
| 40000 | 0.625 | 8.5 | 0.1 | 207 | 77 | 4.27 | 0.0026 |
| 50000 | 0.625 | 10.7 | 0.1 | 207 | 66 | 3.41 | 0.0017 |
| 60000 | 0.625 | 12.8 | 0.1 | 207 | 57 | 2.84 | 0.0013 |
| 70000 | 0.625 | 12.7 | 0.086 | 207 | 49 | 2.44 | 0.00095 |

TABLE 1. Experimental range

## 3. Modelling the flow

### 3.1. *Defining equations*

For a fully developed turbulent pulsating flow in a circular pipe the equation which governs the phase-averaged oscillating component is

$$\rho\frac{\partial\tilde{u}}{\partial t}=-\frac{\partial\tilde{p}}{\partial x}+\frac{1}{r}\frac{\partial}{\partial r}[r(\langle\tau^{(t)}\rangle-\bar{\tau}^{(t)})]+\frac{\mu}{r}\frac{\partial}{\partial r}\left(r\frac{\partial\tilde{u}}{\partial r}\right), \tag{11}$$

where $\langle\tau^{(t)}\rangle=-\rho\langle u'v'\rangle$ is the phase-averaged Reynolds stress and $\bar{\tau}^{(t)}=-\rho\overline{u'v'}$, the time-mean Reynolds stress. In order to solve (11) the oscillation-induced Reynolds stress $\tilde{\tau}^{(t)}$, which is defined as

$$\tilde{\tau}^{(t)}=\langle\tau^{(t)}\rangle-\bar{\tau}^{(t)}, \tag{12}$$

has to be specified. This is done by following Boussinesq's concept of turbulent eddy viscosity. The phase-averaged Reynolds stress then can be written as

$$\langle\tau^{(t)}\rangle=\rho\left\langle\nu_t\frac{\partial u}{\partial y}\right\rangle. \tag{13}$$

If it is assumed that the imposed small oscillation induces a variation of turbulent eddy viscosity $\tilde{\nu}_t$ around its time mean value $\bar{\nu}_t$, the oscillation-induced Reynolds stress is expressed as

$$\tilde{\tau}^{(t)}=\rho\left(\bar{\nu}_t\frac{\partial\tilde{u}}{\partial y}+\tilde{\nu}_t\frac{\partial\bar{u}}{\partial y}\right), \tag{14}$$

if it is assumed that the second-order term $\tilde{\nu}_t(\partial\tilde{u}/\partial y)$ is negligible. The time-mean Reynolds stress is written as

$$\bar{\tau}^{(t)}=\rho\left(\bar{\nu}_t\frac{\partial\bar{u}}{\partial y}\right). \tag{15}$$

### 3.2. *Time-mean flow*

Most previous researchers have found that the time-mean flow is not affected by imposed small-amplitude flow oscillations. Experimental results on wall shear stress

obtained in the present study also support this conclusion. Therefore, the time-mean velocity profile is calculated using the same eddy viscosity $\overline{\nu}_t$ that represents a steady flow. An empirical equation proposed by Reichardt (1951) is used for the prediction of $\overline{\nu}_t$ in the core region:

$$\frac{\overline{\nu}_t}{\nu} = \tfrac{1}{6}\kappa y^+\left(1+\frac{r}{r_0}\right)\left[1+2\left(\frac{r}{r_0}\right)^2\right], \tag{16}$$

where $\kappa$ is the von Kármán constant, 0.4.

In the region close to the wall, the mixing-length theory is used so that

$$\overline{\nu}_t = \overline{l}^2\frac{\mathrm{d}\overline{u}}{\mathrm{d}y}, \tag{17}$$

where $\overline{l}$, the mixing length characterizing the undisturbed flow, is described by the van Driest function,

$$\overline{l} = \kappa y[1-\exp(-\overline{D}_m)]. \tag{18}$$

The term $\overline{D}_m$ is a damping function defined as

$$\overline{D}_m = \frac{y\overline{\tau}^{\frac{1}{2}}}{\rho^{\frac{1}{2}}\nu A}, \tag{19}$$

and $\overline{\tau}$ may be taken as equal to $\overline{\tau}_w$, the time-mean shear stress at the wall. The van Driest damping constant $A$ is 26 for pipe flow.

### 3.3. *Quasi-laminar model for the induced flow oscillation*

The simplest model for the flow involves the assumption that $\tilde{\tau}^{(t)} = 0$. This means that the induced oscillations in a turbulent flow will behave the same as for a laminar pulsating flow, i.e.

$$\frac{\partial\tilde{u}}{\partial t} = -\frac{1}{\rho}\frac{\partial\tilde{p}}{\partial x}+\frac{\nu}{r}\frac{\partial}{\partial r}\left(r\frac{\partial\tilde{u}}{\partial r}\right). \tag{20}$$

This equation has been solved by Sexl (1930) and Uchida (1956) for a pressure gradient with sinusoidal variation in time,

$$-\frac{1}{\rho}\frac{\partial\tilde{p}}{\partial x} = a\cos\omega t. \tag{21}$$

The model is usually assumed to approximate the flow at very high frequencies, for which the spatial variation of the imposed flow oscillation is confined to a very thin layer near the wall where turbulence has negligible effect on the time-averaged flow.

For high frequencies (20) can be rewritten using the distance from the wall, $y$, rather than radial distance, $r$. The scaling of the resulting equation suggests that $\tilde{u}/|\tilde{U}_c|$ is a function of $y^+\omega^{+\frac{1}{2}}$. A consequence of this is that $(|\tilde{\tau}_w|/\overline{\tau}_w)/(|\tilde{U}_c|/\overline{u}^*)$ increases as $\omega^{+\frac{1}{2}}$ and that the phase angle between $\tilde{\tau}_w$ and $\tilde{U}_c$ is constant.

### 3.4. *Quasi-steady approximation*

For the case of very low frequencies a pseudosteady approximation can be made whereby the relation between the instantaneous wall shear stress and the instantaneous centreline velocity is the same as for a steady flow:

$$\tau_w = \tfrac{1}{2}fU_c^2\rho, \tag{22}$$

$$f = A\left(\frac{2r_0U_c}{\nu}\right)^{-n}. \tag{23}$$

For a small-amplitude oscillation

$$\tau_w = \overline{\tau}_w + \tilde{\tau}_w, \tag{24}$$

and

$$U_c = \overline{U}_c + \tilde{U}_c, \tag{25}$$

where $\overline{\tau}_w$ and $\overline{U}_c$ are the wall shear stress and centreline velocity without imposed oscillations. By substituting (24) and (25) into (22) and (23) and neglecting second-order terms in $\tilde{U}_c$ and $\tilde{\tau}_w$ (because of the assumption of a small-amplitude oscillation) the following relation for $\tilde{\tau}_w$ is obtained:

$$\frac{\tilde{\tau}_w}{\overline{\tau}_w} = (2-n)\frac{\tilde{U}_c}{u^*}(\tfrac{1}{2}f)^{\frac{1}{2}}. \tag{26}$$

Equation (26) is strictly applicable to much lower frequencies than were covered by the experiments, for which $\tilde{u}$ is described by a plug-flow relation in the central region of the pipe. The quasi-steady approximation can be applied in a less restrictive way by applying it to (16), (17) and (18) to calculate $\tilde{\nu}_t$ in the same way that a relation for $\tilde{\tau}_w$ was obtained from (22). This formulation is the Model C discussed by Thorsness *et al.* (1978) except that $\tau(y)$, rather than $\tau_w$, is used in (19) to define the van Driest damping coefficient. Model C has an advantage over (26) in that it can be applied over a larger range of frequencies.

If the spatial variation of $\tilde{u}$ is confined to a region where $\overline{\nu}_t$ is defined by (17) and (18) then it follows from the scaling of (11) and the quasi-steady approximation that $\tilde{u}/|\tilde{U}_c|$ is a function of $y^+$ and $\omega^+$, and that $(|\tilde{\tau}_w|/\overline{\tau}_w)/(|\tilde{U}_c|/\overline{u}^*)$ and the phase angle are functions only of $\omega^+$. However if the frequency is small enough that the variation of $\tilde{u}$ extends out to the central part of the flow then the quasi-steady approximation predicts that these variables are also a function of the Reynolds number, as is evident from (26).

### 3.5. *Relaxation model*

As mentioned in §1 strong steady favourable and unfavourable pressure gradients have been found to respectively dampen and enhance turbulence in the viscous wall region. A number of previous investigators (Launder & Jones 1969; Cebeci & Smith 1974; Julien, Kays & Moffat 1969; Loyd, Moffat & Kays 1970) have argued that this behaviour causes the thickness of the viscous wall region to increase in favourable pressure gradients and to decrease in unfavourable ones. They represented this effect by allowing $A$ to be a function of the dimensionless pressure gradient, $p^+ = (\mathrm{d}p/\mathrm{d}x)\nu/\rho u^{*3}$. For small $p^+$,

$$A = \overline{A}(1 + k_1 p^+ + k_2 p^{+2} + \ldots), \tag{27}$$

with $k_1 \approx -30$ and $k_2 \approx 1.54 \times 10^3$. This predicts that $A$ increases for increasing negative values of $p^+$ and decreases with increasing positive values.

For situations in which the pressure gradient is varying rapidly in the flow direction, Launder & Jones (1969), Julian *et al.* (1969), and Loyd *et al.* (1970) have proposed a first-order lag equation whereby the flow close to the wall sees an effective pressure gradient given by the equation

$$\frac{\mathrm{d}\left(\dfrac{\mathrm{d}p}{\mathrm{d}x}\right)_{\mathrm{eff}}}{\mathrm{d}(xu^*/\nu)} = \frac{\left(\dfrac{\mathrm{d}p}{\mathrm{d}x}\right) - \left(\dfrac{\mathrm{d}p}{\mathrm{d}x}\right)_{\mathrm{eff}}}{k_L}, \tag{28}$$

where $k_L$ is a relaxation constant approximately equal to 3000. No physical justification is given, so the merit of this lag equation is to be judged by its usefulness.

Alternative approaches would be to relax the entire Reynolds stress (Shemer 1981; Abrams 1984) or to relax the van Driest damping function, $D_m$ (Abrams & Hanratty 1985). No great difference is noted in results obtained from these three approaches.

The pressure gradient in a pulsating flow varies with time rather than with space. A straightforward application of (28) to this case requires the definition of a convection velocity which characterizes the streamwise propagation of disturbances in the viscous wall region to relate spatial variations to time variations. A convection velocity of $C_x^+ = 15$ has been chosen to take account of this effect. Therefore, the effective damping function for a pulsating flow is defined as

$$\frac{\mathrm{d}\left(\frac{\mathrm{d}p}{\mathrm{d}x}\right)_{\mathrm{eff}}}{\mathrm{d}(tu^{*2}/\nu)} = \frac{\left(\frac{\mathrm{d}p}{\mathrm{d}x}\right) - \left(\frac{\mathrm{d}p}{\mathrm{d}x}\right)_{\mathrm{eff}}}{(k_{\mathrm{L}}/15)}. \tag{29}$$

### 3.6. *Numerical scheme*

Equation (11) was solved numerically by a Crank–Nicolson implicit scheme with variable spatial grid size. Since the oscillation velocity changes rapidly in the wall region and the final goal of the calculation is to find the velocity gradient at the wall, it is necessary to use a very small grid size close to the wall. Grid sizes that are increasing in a geometric series of $Y$ were chosen:

$$Y_j = \frac{\Delta Y_1 (H^{j-1} - 1)}{(H-1)}, \quad 1 < j \leqslant J, \tag{30}$$

where $\Delta Y_1$ is the first grid size near the wall, and factor $H$ is the ratio of two consequent grid sizes. $H$ is chosen as 1.05 for present work.

The first grid size $\Delta Y_1$ was selected small enough that the velocity gradient at the wall can be calculated by the assumption of a linear variation of velocity in that region. After several tries $\Delta Y_1$ was taken as $\frac{1}{30}$ of the Stokes-layer thickness.

The initial condition, time zero, was chosen as the quasi-laminar result, obtained by solving (20) analytically. Equal time steps of $\Delta(\omega t) = \frac{2}{128}\pi$ were used. After about five periods the calculated velocities at each phase of the cycle were found to converge to constant values.

## 4. Results

### 4.1. *Time-averaged properties of the velocity gradient at the wall*

Figure 4 shows the measured time-averaged values of the velocity gradient at the wall at different flow conditions. It is observed that the imposed oscillation has no effect on the time-mean velocity gradient at the wall.

Intensities of turbulent fluctuations of velocity gradient at the wall are shown in figure 5. The intensities are the results of long time averaging, and can be seen to be independent of Reynolds number and of the presence of an imposed flow oscillation. The value, 0.35, agrees with previous measurements by other researchers (Sirkar 1969; Fortuna & Hanratty 1971; Eckelman 1971).

Power spectra of the instantaneous signals are shown in figure 6 for a flow for which the median frequency of the turbulence and the frequency of the imposed oscillation are the same. The sharp peak at a frequency of 0.63 Hz in figure 6(*a*) represents the contribution of the imposed oscillation to the total energy. Figure 6(*b*) shows the spectrum of turbulent fluctuations of velocity gradient at the wall after removing the phase-averaged values from the instantaneous signals. Figure 6(*c*) is the

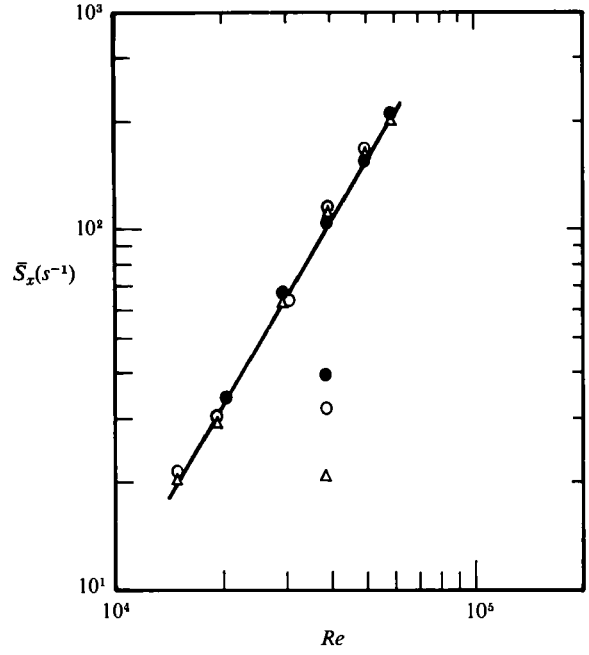


FIGURE 4. Time-averaged velocity gradient at the wall in different flow conditions. ●, steady flow; ○, pulsating flow ($f = 0.325$ Hz); △, pulsating flow ($f = 0.625$ Hz).

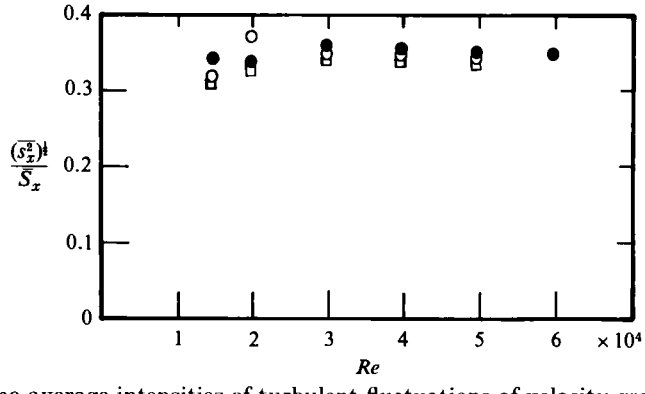


FIGURE 5. Time-average intensities of turbulent fluctuations of velocity gradient at the wall in different flow conditions. ●, steady state; ○, $f = 0.625$ Hz; □, $f = 0.325$ Hz.

spectrum of turbulent fluctuations of the velocity gradient at the wall in steady flow at a Reynolds number of 30000. No major difference is observed between figure 6(*b*) and (*c*).

The peaks at frequencies of 13 and 3 Hz are considered to be caused by some unknown disturbance in the flow system, because the peaks appear at the same frequencies in the steady flow at different Reynolds numbers.

### 4.2. *Phase-averaged values of the velocity gradient at the wall in a pulsating flow*

Figure 7(*a*) shows the phase-averaged pressure gradient measured at a Reynolds number of 15400 using an imposed 0.625 Hz oscillation which has an amplitude that

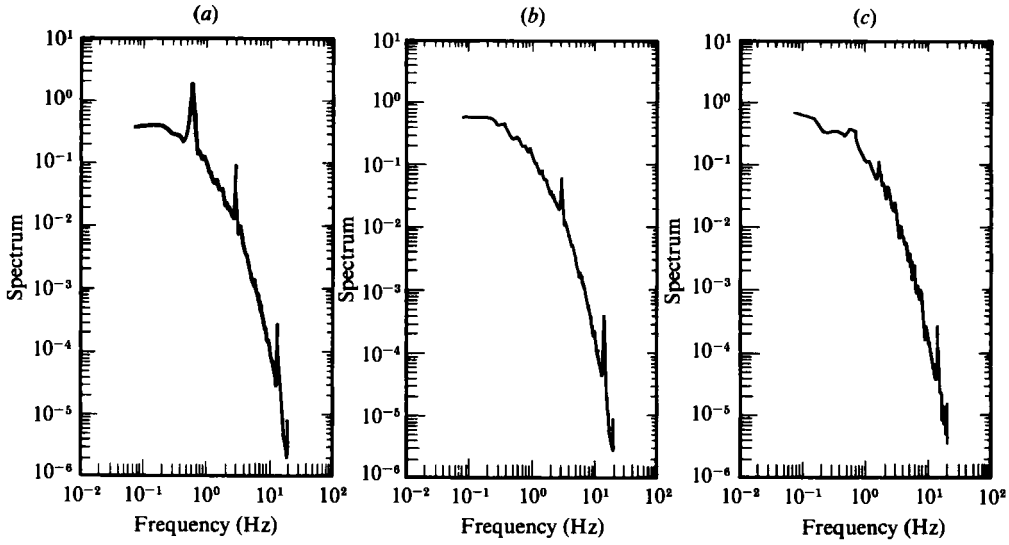


FIGURE 6. Spectrum of fluctuations of velocity gradient at the wall ($Re = 30000$): (*a*) With oscillation $f = 0.62$ Hz; (*b*) after subtracting the oscillation component; (*c*) in steady flow.

is 10% of the central mean velocity. The pressure-gradient variation is normalized with the time-mean pressure gradient. It is seen that the amplitude of pressure-gradient oscillation is very large in this case, about eighty times its mean value. This is caused by the relatively high frequency of the oscillation and the low time-mean velocity. This case represents one extreme in the experimental range, i.e. a low Reynolds number and a high-frequency oscillation. The solid line is the least-square fit of the data with a cosine curve. It is seen that most of the energy of the flow oscillation is contained in a single harmonic.

Figure 7 (*b*) shows the phase-averaged velocity gradient at the wall, normalized with its mean value. The 50% variation of velocity gradient at the wall, compared with the 10% variation of the central velocity, arises because the spatial variation of the oscillation velocity is confined to a thin layer close to the wall for this high-frequency case. The data are fitted quite well with a cosine curve that is shifted about 54° relative to the curve describing the pressure gradient. This indicates a linear response of the phase-averaged flow field to the imposed pressure variation. A linear response is also indicated from experimental results shown in figure 8, which were obtained with a 5% variation of the central velocity. The amplitude of the pressure gradient is about forty times that of the mean and the amplitude of the velocity gradient is one half of that indicated in figure 7 (*b*). The phase shifts of the velocity gradients are the same for both cases.

It is interesting that phase-averaged intensities of turbulent fluctuations are highly nonlinear, as shown in figure 7 (*c*), even though their time average and frequency spectra are the same as in steady flow. This nonlinear effect seems to be related to the amplitude of the imposed oscillation. For example, the nonlinear effect is not so obvious in figure 8 (*c*) as it is in figure 7 (*c*). It is of interest to note that the maximum value of intensity occurs close to when the pressure gradient has its maximum favourable value, and the minimum, close to when the maximum of unfavourable pressure gradient occurs. This contrasts with the finding for boundary-layer flows that turbulence near the wall is suppressed by a favourable pressure gradient and

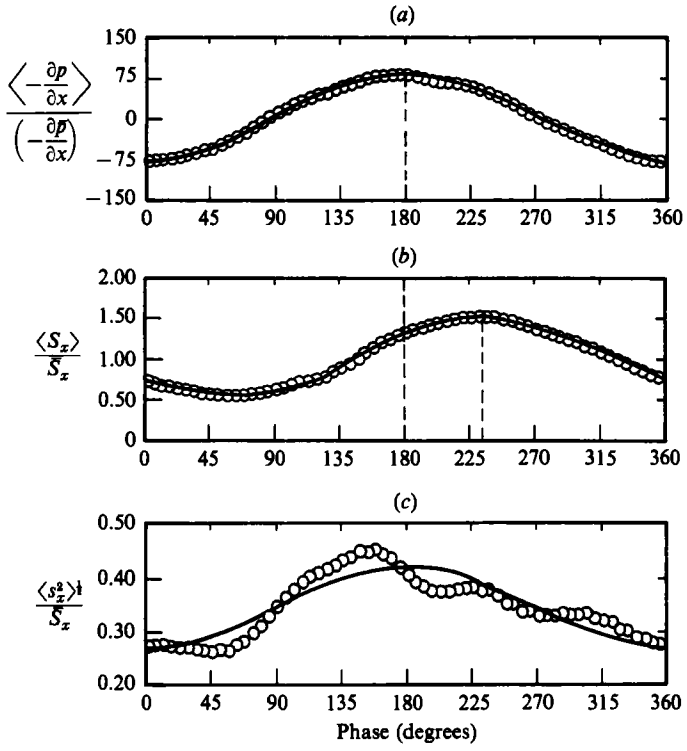


FIGURE 7. Phase-averaged values at $Re = 15400$, $f = 0.625$ Hz and $a = 0.1$ ($\omega^+/15 = 0.014$): (*a*) phase-averaged favourable pressure gradient *vs.* phase; (*b*) phase-averaged velocity gradient at the wall *vs.* phase; (*c*) phase-averaged intensity of velocity gradient at the wall *vs.* phase.

enhanced by an unfavourable one. These results support the argument that the turbulence does not respond immediately to a high-frequency oscillation of the pressure gradient.

Figure 9 shows another set of data at a Reynolds number of 60000 and a frequency of 0.325 Hz. The amplitude of the central velocity oscillation is about 5%. This case represents another extreme in the experimental range; that is a high Reynolds number and a low frequency. In figure 9(*a*), the amplitude of the pressure gradient is seven times its time-mean value and there is some scatter of the data. Phase-averaged measurements of the velocity gradient at the wall are shown in figure 9(*b*). For the same 5% amplitude of central velocity variation, the responses at the wall for the two extremes of the experiments are quite different, as can be seen by comparing figures 8(*b*) and 9(*b*). For example, the amplitude of the velocity gradient is about 6% and the phase shift is 67° in this case, rather than about 25% and 54° in the case of low Reynolds number and high frequency. The intensity data shown in figure 9(*c*) are more scattered. However, a sinusoidal variation can still be distinguished. It is interesting to note that in this case the minimum value of the intensity occurs close to the maximum favourable pressure gradient and the maximum occurs near the maximum of unfavourable pressure gradient. This indicates that high-frequency turbulence that occurs at large Reynolds number can adjust to a slow oscillation of the pressure gradient.

It is also to be noted from figures 8(*c*) and 9(*c*) that the wave-induced variation

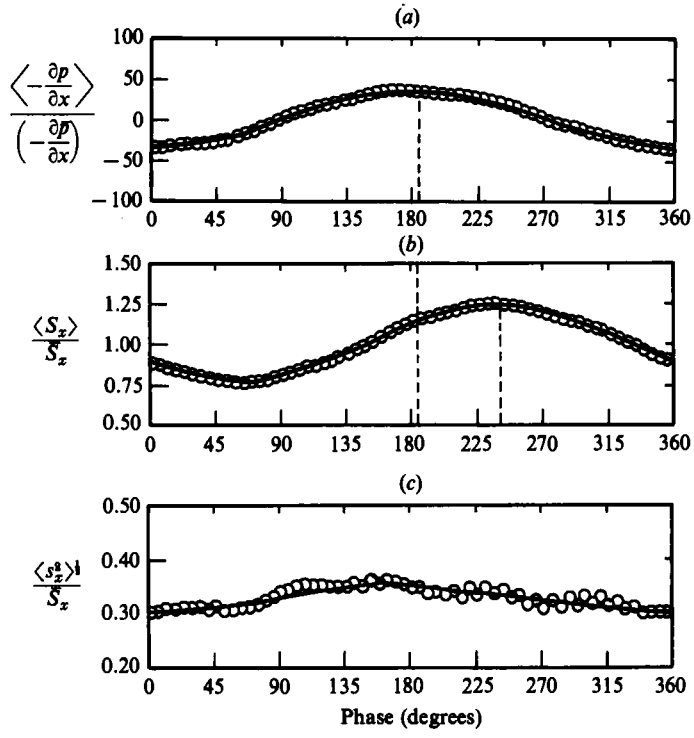


FIGURE 8. Phase-averaged values at $Re = 15400$, $f = 0.625$ Hz and $a = 0.05$ ($\omega^+/15 = 0.014$): (*a*) phase-averaged favourable pressure gradient *vs.* phase; (*b*) phase-averaged velocity gradient at the wall *vs.* phase; (*c*) phase-averaged intensity of velocity gradient at the wall *vs.* phase.

of the intensity of the shear-stress fluctuations increases significantly with an increase of the dimensionless frequency from $\omega^+/15 = 0.00065$ to $\omega^+/15 = 0.014$; however, this is not as much as would be expected from the very large increase of the wave-induced variation of the pressure gradient and the time-averaged velocity gradient at the wall. This is another manifestation of the relaxation phenomenon.

### 4.3. *Amplitude and phase of the velocity gradient at the wall*

Since the velocity gradient at the wall shows a linear response to sinusoidal imposed oscillations of small amplitude, its variation can be characterized by an amplitude and a phase shift relative to the imposed oscillation. Figures 10 and 11 summarize the experimental results obtained under different flow conditions. The phase shifts are plotted relative to the variation of the central velocity, which lags the pressure gradient by 90°, as described in (6). The amplitude $|\tilde{S}_x|/\overline{S}_x$ is normalized by $|\tilde{u}_c|/\overline{u}^*$ to take account of the effect of using different amplitudes of oscillation. The values of $|\tilde{u}_c|$ were not measured but were calculated from the measurements of the time-varying pressure gradient by using equation (5). Thus measurements of the amplitude of the oscillating shear stress were actually normalized with measurements of the amplitude of the oscillating pressure gradient, since $|\tilde{U}_c| = (|\mathrm{d}\tilde{p}/\mathrm{d}x|)/\rho\omega$.

The correlations in figures 10 and 11 are similar to those used by Abrams & Hanratty (1985) to characterize the spatial variation of shear stress along a wavy surface. The abscissa $\omega^+/15$ corresponds to their $\alpha^+ = 2\pi\nu/\lambda u^*$, since the dimensionless turbulence convection velocity in the viscous wall region equals approximately

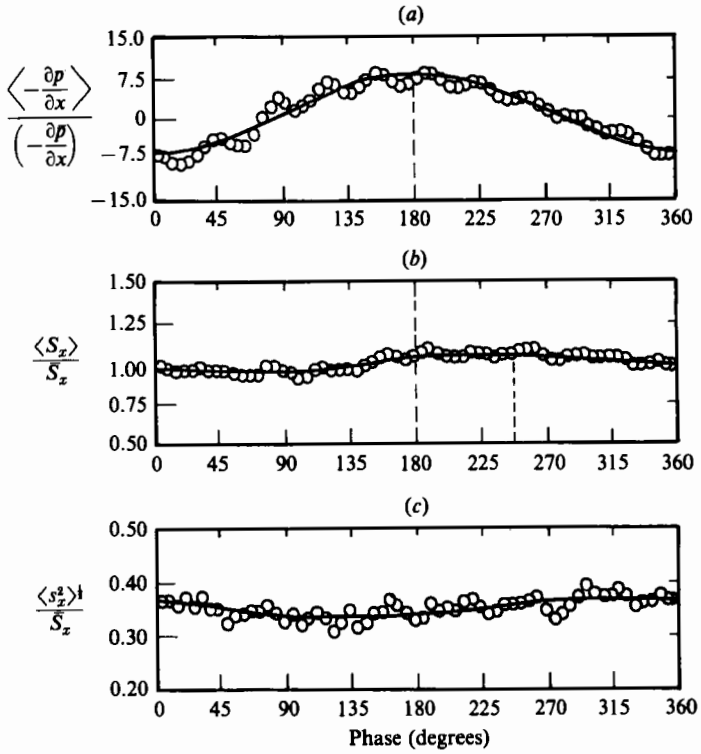


FIGURE 9. Phase-averaged values at $Re = 60000$, $f = 3.25$ Hz and $a = 0.05$ ($\omega^+/15 = 0.00065$): (*a*) phase-averaged favourable pressure gradient *vs.* phase; (*b*) phase-averaged velocity gradient at the wall *vs.* phase; (*c*) phase-averaged intensity of velocity gradient at the wall *vs.* phase.

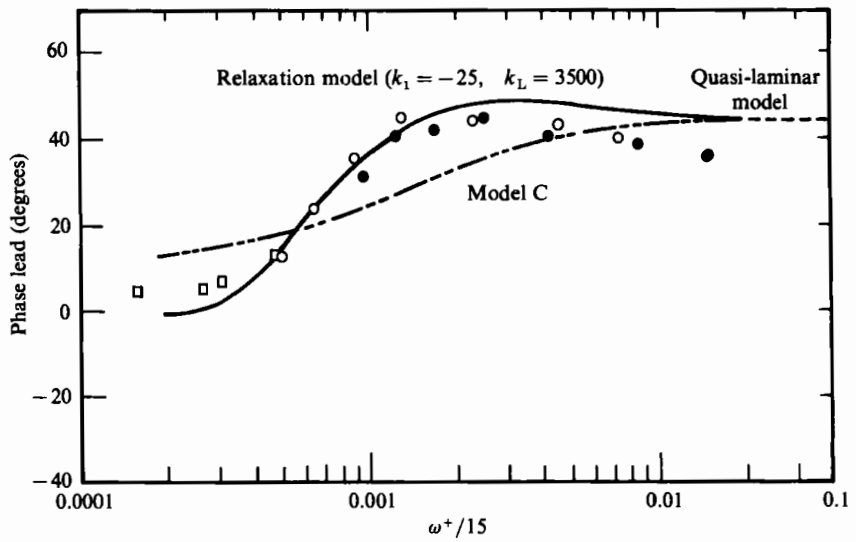


FIGURE 10. Phase lead (relative to the central velocity) of velocity gradient at the wall: ●, $f = 0.625$ Hz; ○, $f = 0.325$ Hz; □, from Ramaprian & Tu (1983).

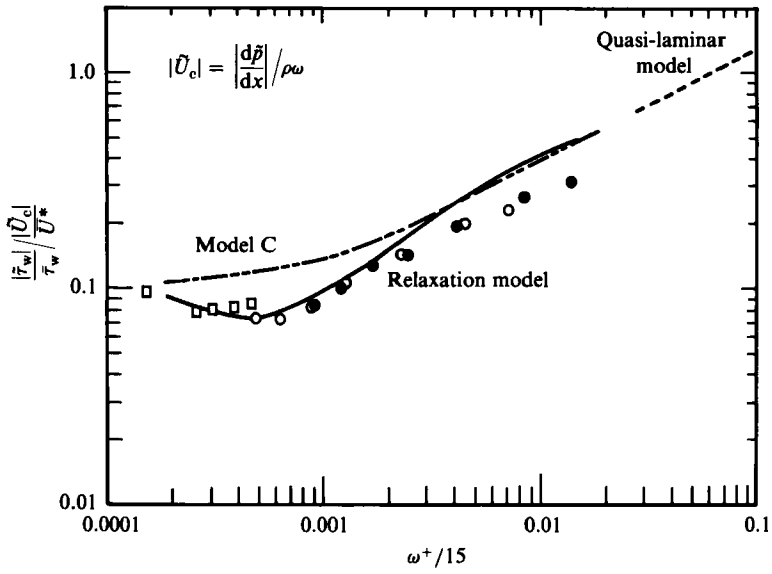


FIGURE 11. Amplitude of velocity gradient at the wall relative to the measured amplitude of the oscillating pressure gradient, since $|\tilde{U}_c| = |d\tilde{p}/dx|/\rho\omega$: ●, $f = 0.625$ Hz; ○, $f = 0.325$ Hz; □, from Ramaprian & Tu (1983).

15. For fixed frequencies, an increase of $\omega^+/15$ corresponds to a decrease of Reynolds number. Consequently, the data show that the phases and amplitudes for fixed frequencies are changing with Reynolds number. It is noted that the results obtained for the two frequencies that were studied fall on the same curves when plotted in the manner shown in figures 10 and 11. For reference, the data obtained by Ramaprian & Tu (1983) are also given.

The curves designated Model C in figures 10 and 11 are obtained from a numerical solution of (11) and (14) by applying a quasi-steady assumption to the turbulent viscosity function for a flat wall, as outlined in §3.4. For very large $\omega^+$ the change $\tilde{u}$ is confined to a region within the viscous wall layer where flat-wall measurements show the turbulent viscosity to be small compared to the molecular viscosity. Consequently Model C gives the same results as the quasi-laminar model for large $\omega^+$.

It is noted that the experimental results shown in figures 10 and 11 disagree with the quasi-steady approximation (Model C). In particular, this approximation does not predict the sharp change in the phase angle in the range $\omega^+/15 = 0.0005$–$0.002$ and gives values of the amplitude of $\tilde{\tau}_w$ which are too large.

The most important result of this paper is the finding that the phase angle characterizing the temporal variation of $\tilde{\tau}_w$ is similar to that found for the spatial variation of $\tau_w$ over a solid wavy surface by Abrams & Hanratty (1985) at $\alpha^+ \approx 0.0005$–$0.0015$. This suggests that the same mechanism is operative and that the two experiments can be compared by using the convection velocity in the viscous wall region.

The solid curves in figures 10 and 11 were calculated using the relaxation model (discussed in §3.5) that provided a good fit to the measurements of Abrams & Hanratty for the shear-stress variation over a wavy surface. This model with $k_1 = -25$ and $k_L = 3500$ appears to be able to represent the amplitude of $\tilde{\tau}$ and the rapid change of phase in the range $\omega^+/15 = 0.0005$–$0.002$.

However, there is a marked difference in the results obtained for large frequencies and for large wavelengths. For $\alpha^+ > 0.002$ the amplitude of the wave-induced variation in $\tau_w$ agrees with predictions based on a quasi-laminar assumption (or on the relaxation model). Experiments using imposed flow oscillations with $\omega^+/15 > 0.002$ give significantly lower results than predicted by a quasi-laminar model.

## 5. Discussion

This paper reports on measurements of the time variation of the phase-averaged wall shear stress caused by the imposition of controlled sinusoidal oscillations on the flow of a turbulent fluid through a pipe. Results are presented for a range of dimensionless frequencies $\omega^+$ higher than had been presented by previous investigators. By using a small amplitude of imposed oscillation a linear response is obtained whereby the wall-shear-stress variation is described by a single harmonic with the same frequency as the imposed oscillation and with an amplitude which varies linearly with the amplitude of the imposed oscillation. The measurements can therefore be characterized by a relative amplitude and a relative phase.

The study used two imposed frequencies and a number of different flow rates so that dimensionless frequencies of $\omega^+ = 0.0075$–$0.21$ were covered. In this range the results are correlated using wall parameters. Apparently much smaller $\omega^+$ are required for the spatial variation of the disturbance velocity to extend far enough away from the wall that pipe Reynolds number is an additional parameter, as suggested by (26). The influence of frequency at high frequencies can, therefore, be studied either by changing the flow rate or by changing the frequency.

The dimensionless frequency is defined as $\omega^+ = (\nu^2/u^{*2})/(\nu/\omega)$ or as $\omega^+ = 2(\delta_v/\delta_s)^2$, where $\delta_v = \nu/u^+$ is the lengthscale of the viscous sublayer and $\delta_s = 2\nu/\omega$ is the thickness of the Stokes layer. Consequently, for $\omega^+ > 0.08$ (or $\omega^+/15 > 0.0053$) the Stokes layer is thinner than the viscous sublayer, and it might be expected that turbulence will have a small effect on the imposed oscillations. However, as already noted, measured amplitudes are much lower for $\omega^+ > 0.08$ than is predicted for a quasi-laminar behaviour. This result was unexpected and is not yet understood.

Considerable work was done (Mao & Hanratty 1985) to examine the frequency response of the wall probes. The consequence of this work is that the possible errors involved in correcting for frequency response are far less than the difference from the quasi-laminar solution shown in figure 11. The measurements of the oscillation-induced variation in the wall shear stress would suggest the possibility that the results could be due to some nonlinear effect. This explanation is ruled out since the same results have been obtained with two different oscillation amplitudes, as shown in figures 6 and 7. Furthermore, measurements of the velocity field very close to the wall by Jayaraman, Parikh & Reynolds (1982) and by Binder & Kueny (1982) also seem to suggest lower oscillation amplitudes at high frequencies than would be calculated by the quasi-laminar model. Consequently, we conclude that oscillation-induced variations of the turbulence in the viscous wall layer, not taken into account by present theories of turbulence, occur in the viscous sublayer at high $\omega^+$. However, these variations appear to have no measurable effect on the time-averaged velocity (figure 4) or on the time-averaged turbulence properties.

It should be noted that the median frequency of the turbulence is $\omega^+/15 \approx 0.004$. Thus, the effect discussed above appears to occur when the imposed oscillation is equal to or greater than the dominant frequency of the turbulence. This result seems

consistent with the suggestion by Mizushina, Maruyama & Shiozaki (1973) that significant changes in the turbulence structure occur when the frequency of the imposed oscillation is the same as the bursting frequency of turbulence.

For $\omega^+/15 < 0.0021$ the dimensionless Stokes-layer thickness is greater than eight wall units, $\delta_s^+ \geqslant 8$. One would not expect a quasi-laminar model to be applicable. The straightforward application of a turbulence model developed for flow over a flat surface (Model C) is not capable of describing the experimental results and, in particular, the sharp change of the phase angle over a rather narrow range of $\omega^+$. However, the use of the relaxation model, which argues that flow-induced oscillations in the pressure gradient can enhance (unfavourable pressure gradient) or dampen (favourable pressure gradient) turbulence in the viscous wall region ($y^+ < 40$), does appear to describe the results. In fact, the parameters, $k_1 = -25$ and $k_L = 3500$, chosen to fit the experimental results are close to those used by Loyd *et al.* (1970) to describe boundary-layer flows and by Abrams & Hanratty (1985) to describe flow over a wavy surface.

According to this model the sharp change in phase angle is associated with a relaxation phenomenon whereby the turbulence does not respond immediately to the oscillation-induced variation of the pressure gradient. Some support for this interpretation is obtained from the measurements of the oscillation-induced variation of the mean-square values of the turbulence fluctuations in the wall shear stress. At low $\omega^+$ it is almost in phase with an unfavourable pressure gradient while at high $\omega^+$ it is almost in phase with a favourable pressure gradient (see figures 7 and 9).

This work was supported by the Office of Naval Research under grant N00014-88-82-12-0324 and by the Shell Companies Foundation.

## REFERENCES

ABRAMS, J. 1984 Turbulent flow over small amplitude solid waves. Ph.D. thesis, University of Illinois, Urbana.

ABRAMS, J. & HANRATTY, T. J. 1985 Relaxation effects observed for turbulent flow over a wavy surface. *J. Fluid Mech.* **151**, 443–455.

BENDAT, J. S. & PIERSOL, A. G. 1971 *Random Data: Analysis and Measurement Procedures.* Wiley.

BINDER, G. & KUENY, J. L. 1982 Measurements of the periodic velocity oscillations near the wall in unsteady turbulent channel flow. In *Turbulent Shear Flows 3* (ed. L. J. S. Bradbury, F. Durst, B. E. Launder, F. W. Schmidt, J. H. Whitelaw), pp. 6–17, Springer-Verlag.

BINDER, G., TARDU, S., BLACKWELDER, R. F. & KUENY, J. L. 1985 Large amplitude periodic oscillations in the wall region of a turbulent channel flow. *Fifth Symp. on Turbulent Shear Flows, Cornell University, Ithaca, New York* (ed. L. J. S. Bradbury, B. E. Launder, F. W. Schmidt, J. H. Whitelaw). Springer.

CARR, L. W. 1981 A review of unsteady turbulent boundary-layer experiments. In *Unsteady Turbulent Shear Flows* (ed. R. Michel, J. Cousteix & R. Houdeville), pp. 3–34. Springer.

CEBECI, T. & SMITH, A. M. O. 1974 *Analysis of Turbulent Boundary Layers.* Academic.

ECKELMAN, L. D. 1971 The structure of wall turbulence and its relation to eddy transport. Ph.D. thesis, University of Illinois, Urbana.

FORTUNA, G. & HANRATTY, T. J. 1971 Frequency response of the boundary layer on wall transfer probes. *Intl J. Heat Mass Transfer* **14**, 1499–1507.

HANRATTY, T. J. & CAMPBELL, J. A. 1983 Measurement of wall shear stress. In *Fluid Mechanics Measurements* (ed. R. J. Goldstein), pp. 559–615. Hemisphere.

HANRATTY, T. J., CHORN, L. G. & HATZIAVRAMIDIS, D. T. 1977 Turbulent fluctuations in the viscous wall region for Newtonian and drag reducing fluids. *Phys. Fluids* **20**, S112–119.

HUSSAIN, A. K. M. F. & REYNOLDS, W. C. 1970 The mechanics of a perturbation wave in turbulent shear flow. *Stanford University Thermosci. Div. Tech. Rep.* FM-6.

JAYARAMAN, R., PARIKH, P. & REYNOLDS, W. C. 1982 An experimental study of the dynamics of an unsteady turbulent boundary layer. *Stanford University Thermosci. Div. Tech. Rep.* TF-18.

JULIEN, H. L., KAYS, W. M. & MOFFAT, R. J. 1969 The turbulent boundary over a porous plate: experimental hydrodynamics of favorable pressure gradient flows. *Stanford University Thermosci. Div. Tech. Rep.* HMT-4.

LAUNDER, B. E. & JONES, W. P. 1969 Sink flow turbulent boundary layers. *J. Fluid Mech.* **38**, 817.

LOYD, R. J., MOFFAT, R. J. & KAYS, W. M. 1970 The turbulent boundary layer on a porous plate: an experimental study of the fluid dynamics with strong favorable pressure gradients and blowing. *Stanford University Thermosci. Div. Tech. Rep.* HMT-13.

MAO, Z.-X. 1984 Studies of the wall shear stress in a turbulent pulsating pipe flow. Ph.D. thesis, University of Illinois at Champaign-Urbana.

MAO, Z.-X. & HANRATTY, T. J. 1985 The use of scalar transport probes to measure wall shear stress in a flow with imposed oscillations. *Exp. Fluids* **2**, 129–135.

MIZUSHINA, T., MARUYAMA, T. & SHIOZAKI, Y. 1973 Pulsating turbulent flow in a tube. *J. Chem. Engng Japan* **6**, 487–494.

RAMAPRIAN, B. R. & TU, S. W. 1983 Fully developed periodic turbulent pipe flow. Part 2. The detailed structure of the flow. *J. Fluid Mech.* **137**, 59–81.

REICHARDT, J. 1951 Die Grundlagen des Turbulenten Wärmeüberganges. *Arch. Ges. Warmetechnik* **2**, 129–143.

REYNOLDS, W. C. 1974 Recent advances in the computation of turbulent flows. *Adv. Chem. Engng* **9**, 193–246.

REYNOLDS, W. C. 1976 Computation of turbulent flows. *Ann. Rev. Fluid Mech.* **8**, 183–208.

SEXL, TH. 1930 Über den von E. G. Richardson Entdeckten Annulareffekt. *Z. Phys.* **61**, 349.

SHEMER, L. 1981 Investigation of the turbulent characteristics of a pulsating pipe flow. Ph.D. thesis, Tel Aviv University, Israel.

SIRKAR, K. K. 1969 Turbulence in the immediate vicinity of a wall and fully developed mass transfer at high Schmidt numbers. Ph.D. thesis, University of Illinois at Champaign-Urbana.

SIRKAR, K. K. & HANRATTY, T. J. 1970 The limiting behaviour of the turbulent transverse velocity component close to a wall. *J. Fluid Mech.* **44**, 605–614.

THORSNESS, C. B., MORRISROE, P. E. & HANRATTY, T. J. 1978 A comparison of linear theory with measurements of the variation of shear stress along a solid wave. *Chem. Engng Sci.* **33**, 579–592.

UCHIDA, S. 1956 The pulsating viscous flow superposed on the steady laminar motion of incompressible fluid in a circular pipe. *Z. angew. Math. Phys.* **7**, 403–421.